Sampling in cylindrical 2D PET

Yannick Grondin, Laurent Desbat, Michel Desvignes

Sampling in cylindrical 2D PET

Yannick Grondin[(1,2)], Laurent Desbat[(1)] and Michel Desvignes[(2)]
(1) TIMC-IMAG, UMR CNRS 5525, UJF-Grenoble 1 (GU) In^{3}S, Faculté de Médecine, 38706 La Tronche France
(2) Grenoble-INP/Phelma/ GIPSA-LAB
961 Rue de la houille blanche BP 46 St Martin d'Heres France
Yannick.Grondin@imag.fr, Laurent.Desbat@imag.fr, michel.desvignes@gipsa-lab.inpg.fr

Abstract:

In this paper, we study 2D cylindrical Positron Emission Tomography (2D PET) sampling. We show that rectangular sampling schemes are more efficient than usual square schemes.

1. PET and sampling

1.1 PET

The aim of Positron Emission Tomography (PET) is to map the internal nuclear activity of a patient from exterior measurement. Usually, the patient received some nuclear substance by inhalation or injection. In PET this substance is tagged with a radioactive isotope, such as Carbon-11, Fluorine-18, Oxygen-15. This substance has also chemical and biological properties that enable to visualize metabolism and functions of patient organs (such as blood flow). This substance, called radiotracer, emits a positron per decay. The positron annihilates with an electron, which results in the emission of two opposite gamma rays detected in a PET system. Thanks to detectors surrounding the patient and a powerful electronic processing, coincident photon pairs can be sorted, meaning that the emission occurred on the line joining both detectors.

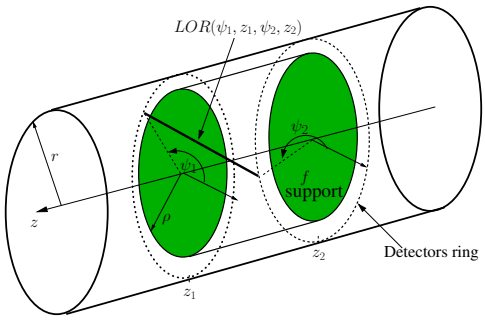

Figure 1: Parametrization of a LOR with the variables $(\psi_1, z_1, \psi_2, z_2)$.

In a cylindrical PET system of radius r, see Fig. 1, the unitary detectors are distributed on a cylinder surrounding the patient (supposed to lie in a cylinder of radius ρ). Each gamma ray detector localization can be parametrized by cylindrical coordinates (ψ, z). When the coincidence on two detectors (ψ_1, z_1) and (ψ_2, z_2) is detected, one knows that some activity occurs on the line joining the detectors (ψ_1, z_1) and (ψ_2, z_2). This line is called a LOR (Line Of Response).

In 2D mode, lead rings called septa, see Fig. 2, are used to restrict detected LORs to be essentially perpendicular to the PET cylinder axis. In this case, LORs have only three parameters (ψ_1, ψ_2, z), see Fig. 3. LORs with a small oblicity (crossed LORs) are usually approximated to LORs perpendicular to the axis, between two true detectors rings, creating a virtual detection ring, allowing to improve the sampling rate along the axis direction, see Fig. 2.

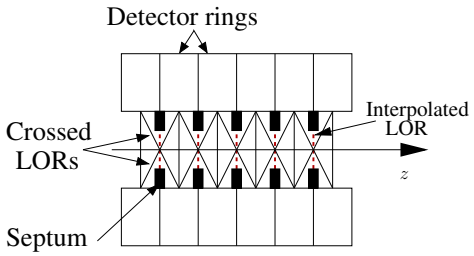

Figure 2: Crossed LORs interpolated to improve axial sampling .

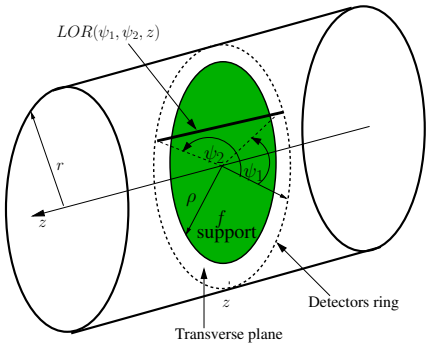

Figure 3: Parametrization of a LOR with the variables (ψ_1, ψ_2, z).

In 2D PET, after the attenuation correction [5] the measure can be modeled by $g : [0, 2\pi] \times [0, 2\pi] \times \mathbb{R} \to \mathbb{R}$, with

$$g(\psi_1, \psi_2, z) = \int_{\mathbb{R}} f(u(\psi_1, z) + t\theta(\psi_1, \psi_2))\, dt$$

with $u(\psi_1, z) = (r\cos\psi_1, r\sin\psi_1, z)^t$ and $\theta(\psi_1, \psi_2) =$

$\frac{1}{2\left|\sin\left(\frac{\psi_1-\psi_2}{2}\right)\right|}(\cos\psi_2-\cos\psi_1,\sin\psi_2-\sin\psi_1,0)^t$. Obviously g satisfies the symmetry relation

$$g(\psi_1,\psi_2,z)=g(\psi_2,\psi_1,z). \tag{1}$$

1.2 Sampling

We want to sample a function g being 2π-periodic in its two first variables and in $\mathbb{R}$ in its third variable. This is a particular case of the general framework of sampling of function on groups, see for example [2, 3]. In this case, the Fourier transform of $g\in C_0^\infty([0;2\pi[\times[0;2\pi[\times\mathbb{R})$ can be defined by:

$$\hat{g}(\xi)=\frac{1}{(2\pi)^2\sqrt{2\pi}}\int_{[0;2\pi[}\int_{[0;2\pi[}\int_{\mathbb{R}}g(x)e^{-ix\cdot\xi}dx,$$

where $x=(\psi_1,\psi_2,z)^t\in[0;2\pi[\times[0;2\pi[\times\mathbb{R}$, $\xi=(p_1,p_2,\zeta)^t\in\mathbb{Z}\times\mathbb{Z}\times\mathbb{R}$ and $\xi\cdot x=p_1\psi_1+p_2\psi_2+\zeta z$. The inverse Fourier transform defined for G a function on $\mathbb{Z}\times\mathbb{Z}\times\mathbb{R}$ is given by

$$\begin{aligned}\check{G}(x)&=\frac{1}{\sqrt{2\pi}}\int_{\mathbb{Z}\times\mathbb{Z}\times\mathbb{R}}G(\xi)e^{ix\cdot\xi}\\&=\frac{1}{\sqrt{2\pi}}\sum_{p_1\in\mathbb{Z}}\sum_{p_2\in\mathbb{Z}}\int_{\zeta\in\mathbb{R}}G(p_1,p_2,\zeta)e^{i(p_1\psi_1+p_2\psi_2+\zeta z)}d\zeta.\end{aligned}$$

Let $\mathbf{K}\subset\mathbb{Z}\times\mathbb{Z}\times\mathbb{R}$, the non-overlapping Shannon condition associated to $\mathbf{K}$ for the sampling lattice $L_W=W\mathbb{Z}^3\cap([0;2\pi[\times[0;2\pi[\times\mathbb{R})$ generated by the non singular 3×3 matrix W is that *the sets* $\mathbf{K}+2\pi W^{-t}l, l\in\mathbb{Z}^3$ *are disjoint sets in* $\mathbb{Z}\times\mathbb{Z}\times\mathbb{R}$. The Petersen-Middleton theorem [6, 3] yields the Fourier interpolation formula

$$(S_Wg)(x)=\frac{1}{\sqrt{2\pi}}|\det W|\sum_{y\in L_W}g(y)\check{\chi}_{\mathbf{K}}(x-y),$$

where $\chi_{\mathbf{K}}$ is the indicator function of the set $\mathbf{K}$. The interpolation error is given by

$$||S_Wg-g||_\infty\le\frac{2}{\sqrt{2\pi}}\int_{\xi\notin\mathbf{K}}|\hat{g}(\xi)|d\xi.$$

Thus if $\mathbf{K}$ is the essential support of $\hat{g}$, i.e., $\int_{\xi\notin\mathbf{K}}|\hat{g}(\xi)|d\xi$ can be negligible, then the interpolation error is low. The geometry of the set $\mathbf{K}$ can be exploited for the design of efficient sampling schemes, i.e., the choice of W satisfying the Shannon condition with $|\det W|$ maximal in order to minimize the number of sampling points.

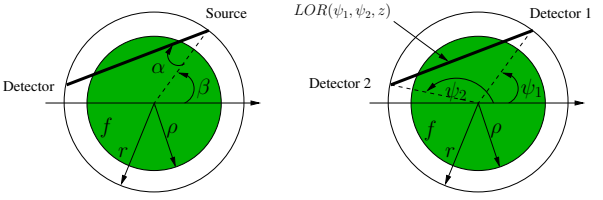

Figure 4: Fan beam (a) and natural PET (b) parametrization in a transverse plane .

2. 3D Sampling in cylindrical PET 2D mode

In [1] we have established the sampling conditions of the 3D Fan-Beam X-ray Transform (3DFBXRT):

$$\mathcal{D}_{e_3{}^\perp}f(\beta,\alpha,z)=\int_{L_{\beta,\alpha,t}}f(u)du,$$

where $u\in\mathbb{R}^3$, $L_{\beta,\alpha,z}$ is the line in the plane perpendicular to e_3 at abscissa z ($z\in\mathbb{R}$), joining the source at $r(\cos\beta,\sin\beta,0)^t+ze_3$, $\beta\in[0,2\pi[$ and the detector at angular position $\alpha\in[-\pi/2,\pi/2[$, see Fig. 4. This geometry appears in X-ray CT scanner when considering the reconstruction of many 2D slices. Cylindrical PET in 2D mode can be linked with the 3DFBXRT in the following way:

$$g(x)=D_{3D}f(\mathbf{A}(x-e_\pi)) \tag{2}$$

where $x=(\psi_1,\,\psi_2,\,z)^t$, $e_\pi=(0,\,\pi,\,0)^t$, and

$$\mathbf{A}=\begin{pmatrix}1&0&0\\-\frac{1}{2}&\frac{1}{2}&0\\0&0&1\end{pmatrix}$$

see Fig 4.

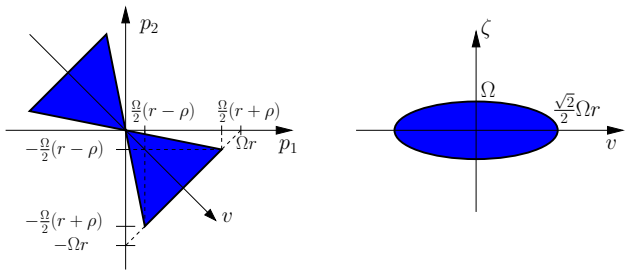

Figure 5: K_g: essential support of $\hat{g}$ for $\eta=\rho/r=2/3$, slices in the planes (p_1,p_2) (left) and (v,ζ) (right). The 3D set K_g is just at the intersection of two cylinders of respective basis the slices in the (p_1,p_2) and (v,ζ) and respective axis ζ and the direction perpendicular to (v,ζ) .

This link allows to easily estimate the essential support of $\widehat{g}:\mathbb{Z}\times\mathbb{Z}\times\mathbb{R}\to\mathbb{R}$. Indeed,

$$\begin{aligned}\widehat{g}(\xi)&=\int_{[0;2\pi[}\int_{[0;2\pi[}\int_{\mathbb{R}}g(x)e^{-ix\cdot\xi}dx\\&=\int_{[0;2\pi[}\int_{[0;2\pi[}\int_{\mathbb{R}}D_{3D}f(\mathbf{A}(x-e_\pi))e^{-ix\cdot\xi}dx\\&=\int_{[0;2\pi[}\int_{[0;2\pi[}\int_{\mathbb{R}}D_{3D}f(\mathbf{A}x)e^{-ix\cdot\xi+ip_2\pi}dx\\&=\frac{(-1)^{p_2}}{|\det\mathbf{A}|}\int_{[0;2\pi[}\int_{[0;2\pi[}\int_{\mathbb{R}}D_{3D}f(x)e^{-i(\mathbf{A^{-1}}x)\cdot\xi}dx\\&=\frac{(-1)^{p_2}}{|\det\mathbf{A}|}\int_{[0;2\pi[}\int_{[0;2\pi[}\int_{\mathbb{R}}D_{3D}f(x)e^{-ix\cdot\left(\mathbf{A^{-t}}\xi\right)}dx\\&=\frac{(-1)^{p_2}}{|\det\mathbf{A}|}\widehat{D_{3D}f}(\mathbf{A^{-t}}(\xi))\end{aligned}$$

From this link we see that the essential support of $\widehat{g}$ is simply a linear transformation of the essential support of

$\widehat{D_{3D}f}$. From [1] it can be easily shown that K_g, the essential support of $\hat{g}(p_1, p_2, \zeta)$ when the emission function f is supposed the be essentially Ω band limited, is given by

$$K_g = \{(p_1, p_2, \zeta) \in \mathbb{Z} \times \mathbb{Z} \times \mathbb{R}, \\ |p_1 - p_2|^2 + r^2\zeta^2 < \Omega^2 r^2; r|p_1 + p_2| < \rho|p_1 - p_2|\}$$

see Fig. 5 for a representation.
The angles ψ_1 and ψ_2 parametrize the same detector ring, thus their sampling must be identical. We consider here only standard sampling, i.e. equidistant sampling along each direction. The most efficient diagonal matrix satisfying the non overlapping Shannon conditions, see Fig. 6, is given by:

$$2\pi \mathbf{W_S^{-t}} = \Omega \begin{pmatrix} r & 0 & 0 \\ 0 & r & 0 \\ 0 & 0 & 2 \end{pmatrix}, \mathbf{W_S} = \frac{2\pi}{r\Omega} \begin{pmatrix} 1 & 0 & 0 \\ 0 & 1 & 0 \\ 0 & 0 & \frac{r}{2} \end{pmatrix} \quad (3)$$

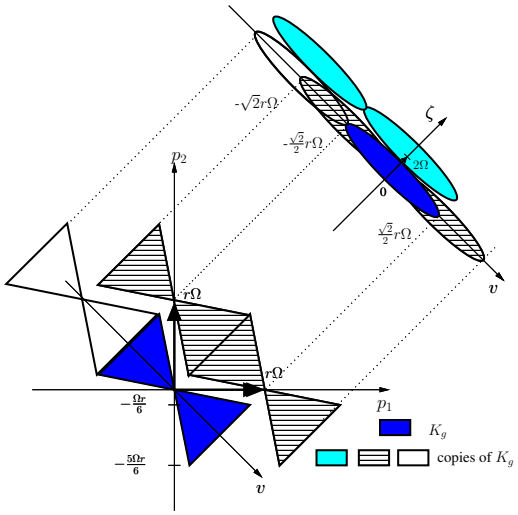

Figure 6: Non overlapping conditions for the rectangular sampling scheme .

Thus we see that the most efficient sampling distances are $\Delta\psi_1 = 2\pi/r\Omega (= \Delta\psi_2)$ and $\Delta z = \pi/\Omega$. $l_z = \Delta z$ would thus be the detector axial length. If we approximate the detector tangential length by $l_t = r\Delta\psi_1$, we see that the most efficient relation is $l_z = l_t/2$, thus the most efficient detectors from the sampling point of view are rectangular detectors. The empirical ring oversampling by rebinning the crossed LORs as in Fig. 2 yields exactly the factor 2 of oversampling in the direction z needed for efficient sampling. This is a theoretical justification of this widely used heuristic rebinning method.

3. Numerical experiments

3.1 Essential support

We have computed from numerical phantom the essential support of $|\hat{g}(p_1, p_2, \zeta)|$ see Fig. 7. In (a) and (c) the simulation is based on simple line integrals of a phantom f built with 3 concentric weighted ball indicator functions: $f = \chi_{B(c,0.03)} + \chi_{B(c,0.05)} + \chi_{B(c,0.07)}$ where $\chi_{B(c,r)}$ is the indicator function of the ball of radius r centered on $c = (0.9, 0, 0)$. The data are simulated for a PET of radius 1.5 with 32 rings and 300 detectors on each ring. (b) and (d) are based on a Monte Carlo (MC) simulation computed with GATE [4]. The phantom f is built with 5 concentric weighted ball sources (of radius r expressed in mm): $f = a(\chi_{B(c,9)} + \chi_{B(c,10)} + \chi_{B(c,11)} + \chi_{B(c,12)} + \chi_{B(c,13)})$, where the center $c = (130, 0, 0)$ mm and the activity $a = 10^6$ becquerel. The data are simulated for a PET of radius 402 mm with 32 rings and 576 detectors on each ring, imitating the ECAT EXACT HR$^+$ scanner of CTI/Siemens. We see that the simulation data are in good agreement with the theoretical results.

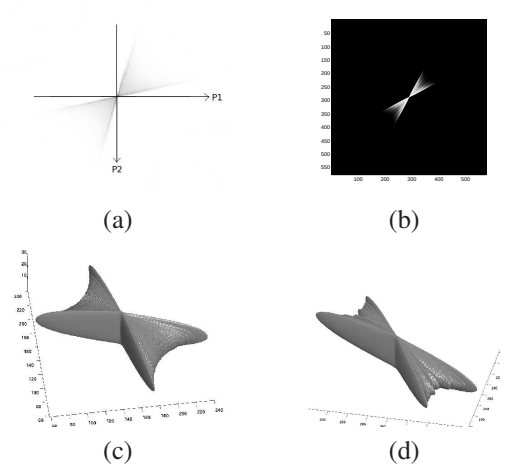

Figure 7: In (a) and (c) the emission function f is the sum of 3 concentric indicator functions. In (b) and (c) the data are obtained by a MC simulation of 5 concentric spherical sources. (a) and (b) slice $\zeta = 0$ of $|\hat{g}(p_1, p_2, \zeta)|$; (c) and (d) 3D visualization of the isosurface at 1% of maximum of $|\hat{g}(p_1, p_2, \zeta)|$ ($|\hat{g}(p_1, p_2, \zeta)|$ is essentially negligible outside of this surface) .

3.2 Reconstruction resolution

In Fig. 8, Fig. 9 and 10, we present the reconstruction of the clock phantom, see [8], from simple line integrals. The simulated cylindrical PET is of radius $r = 1.5$, the reconstruction region is of radius $\rho = 1$. We consider two sampling schemes with essentially the same number of data. The square scheme is based on square detectors, with $l_t = l_z = 0.049$. The number of ring is 20. The number of detectors on a ring is 190. The rectangular scheme is based on rectangular detectors, with $l_t = 2l_z = 0.062$. The number of ring is 32. The number of detectors on a ring is 150. We see in these numerical experiments that the rectangular scheme yields better reconstructions than the square scheme.

4. Conclusion

We have shown the efficiency of the rectangular sampling scheme over the square scheme in 2D mode cylindrical PET. Sampling conditions in fully 3D PET as initiated in [7] are now being investigated.

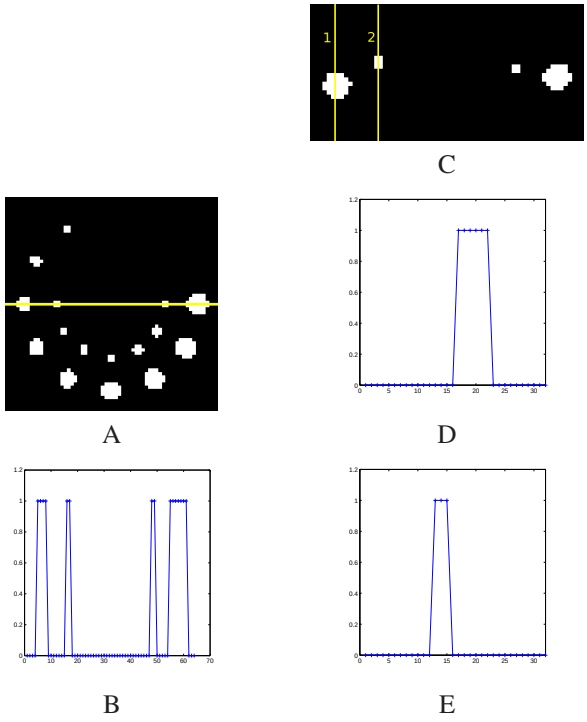

Figure 8: A = Original image: transverse view ; B = Image profile ; C = Original image: axial view ; D = Image profile 1 ; E = Image profile 2 .

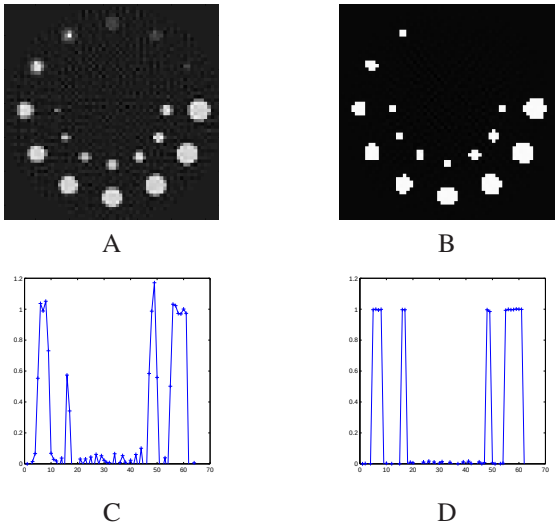

Figure 9: A = Square scheme image: transverse view ; B = Rectangular scheme image: transverse view ; C = Square scheme image profile ; D = Rectangular scheme image profile .

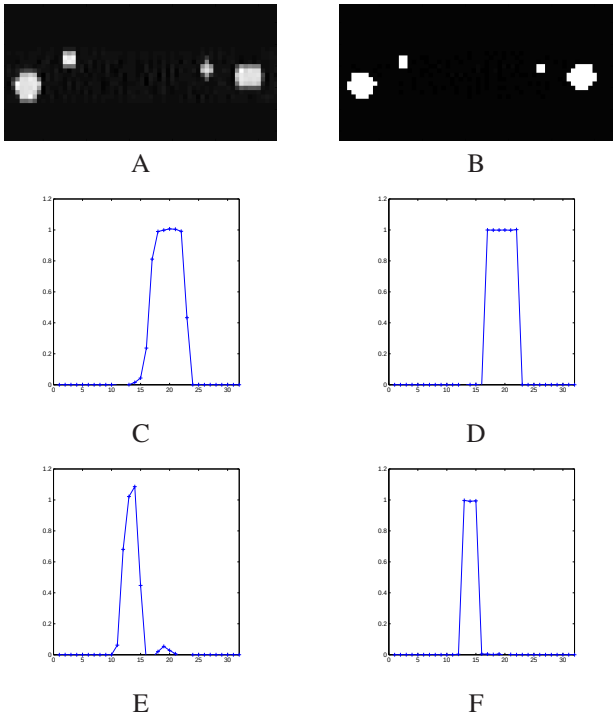

Figure 10: A = Square scheme image: axial view ; B = Rectangular scheme image: axial view ; C = Square scheme image profile 1 ; D = Rectangular scheme image profile 1 ; E = Square scheme image profile 2 ; F = Rectangular scheme image profile 2 .

References:

[1] L. Desbat, S. Roux, P. Grangeat, and A. Koenig. Sampling conditions of 3D Parallel and Fan-Beam X-ray CT with application to helical tomography. *Phys. Med. Biol.*, 49(11):2377–2390, 2004.

[2] A. Faridani. An application of a multidimensional sampling theorem to computed tomography. In *AMS-IMS-SIAM Conference on Integral Geometry and Tomography*, volume 113, pages 65–80. Contemporary Mathematics, 1990.

[3] A. Faridani. A generalized sampling theorem for locally compact abelian groups. *Math. Comp.*, 63(207):307–327, 1994.

[4] S. Jan and coll. Gate: a simulation toolkit for pet and spect. *Phys. Med. Biol*, 49:4543–4561, 2004.

[5] F. Natterer. *The Mathematics of Computerized Tomography*. Wiley, 1986.

[6] D.P. Petersen and D. Middleton. Sampling and reconstruction of wavenumber-limited functions in N-dimensional euclidean space. *Inf. Control*, 5:279–323, 1962.

[7] T. Rodet, J. Nuyts, M. Defrise, and C. Michel. A study of data sampling in pet using planar detectors. In *IEEE Nuclear Science Symp. Conf. Rec*, 2003.

[8] Henrik Turbell. *Cone-Beam Reconstruction Using Filtered Backprojection*. PhD thesis, Linkping University, 2001.